Large-scale structures and molecular mixing

James E. BroadwellM. Godfrey Mungal

Citation: Physics of Fluids A: Fluid Dynamics **3**, 1193 (1991); doi: 10.1063/1.858048
View online: http://dx.doi.org/10.1063/1.858048
View Table of Contents: http://aip.scitation.org/toc/pfa/3/5
Published by the American Institute of Physics

Large-scale structures and molecular mixing

James E. Broadwell
Graduate Aeronautical Laboratories, California Institute of Technology, Pasadena, California 91125
M. Godfrey Mungal
Department of Mechanical Engineering, Stanford University, Stanford, California 94305

(Received 28 August 1990; accepted 20 December 1990)

Scalar mixing and chemical reactions in turbulent shear layers and jets are examined with emphasis on experimental results of high spatial and temporal resolution. Such measurements show that the notion of distinguishing fluids that are molecularly mixed from those that are simply stirred is valid and useful. Two models that seem especially suitable for implementing mixing analyses from this viewpoint are described and speculations on possible connections with the idea of chaotic advection offered.

I. INTRODUCTION

A paragraph taken from Ref. 1, by Aref and Jones, will make clear that the title of this Symposium, *The Fluid Mechanics of Stirring and Mixing*, contains, by implication, many of the major points that we wish to make in this paper. They write the following:

"For convenience we shall follow a terminology suggested by Eckart in which *stirring* signifies the mechanical process whereby fluids are distributed more uniformly within a given domain, i.e., stirring is a process of stretching of intermaterial area. *Mixing*, on the other hand, is the process of diffusion of substances across intermaterial surfaces. Stirring can promote mixing by creating more intermaterial surface area. Mixing depends on material properties, such as diffusivities, whereas stirring is a purely kinematical aspect dependent on flow parameters. Indeed, it is possible to stir fluids that do not mix at all."

A primary objective of this paper is to show that scalar mixing in free turbulent shear flows is well described in these terms and that it is the existence of large-scale structures in these flows that makes such a description useful. More specifically, evidence is cited showing that (1) large-scale motions associated with the structures lead to mean concentration distributions that differ markedly from those of the mean mixed fluid, and (2) the overall mixing rate is influenced by the value of the molecular diffusivities even at what are considered to be high Reynolds numbers.

In the paper, we follow the advice of Leonardo da Vinci, who wrote "Remember, when discoursing about water, to induce first experience, then reason." Today this would perhaps be written as follows: In discussing turbulence, consider first experiment, physical or numerical, and then theory. The paper, consists therefore, mainly of discussions of experimental results and their implications concerning the path to the molecularly mixed state. The paper includes, nevertheless, a discussion of models of this path and some speculations about the relevance of the ideas from chaotic advection to stirring and mixing in turbulent shear flows. For simplicity, only constant, or near constant, density flows are considered. Likewise, though many of the ideas apply to other free shear flows such as wakes and jets in cross flow, only jets and shear layers will be discussed.

The outline of the remainder of the paper is as follows. In Sec. II evidence of the persistence of structures to high Reynolds numbers is presented. In Sec. III scalar mixing and chemical reaction experiments are described. In Sec. IV two models are discussed: a two-stage Lagrangian model; and the linear eddy model. Section V contains speculations about shear flow mixing and chaotic advection and Sec. VI contains some concluding remarks.

II. EVIDENCE OF PERSISTENCE OF STRUCTURES TO HIGH REYNOLDS NUMBERS

This section is a short review of some of the evidence for the existence of large-scale structures in shear flows. We begin first with the findings in two-dimensional mixing layers and conclude with the observations for jets. Of particular interest is the persistence of large-scale motions to high Reynolds numbers.

A. Shear layers

Perhaps the most important photo for evidence of large-scale structures in mixing layers was also the first. Most readers are familiar with the classic shadowgraph photos of Brown and Roshko[2] of the mixing layer formed between a high-speed stream of helium–argon and an equal density, low-speed stream of nitrogen. Their photos clearly show the two-dimensional rollers as well as the fine-scale structure which exist throughout the mixed fluid regions. An important point to note here is that their photos are of the *scalar* field, and not the velocity field. As will be seen in Sec. III, the sharp edges in the visualizations are consistent with the concentration fields to be described later. Such edges are not present in the velocity field.

The issue of existence of the organized structure at high Reynolds number was addressed by several researchers, including Dimotakis and Brown[3] using water as the working medium and Mungal *et al.*[4] using high-speed gases. More recent evidence of the Brown–Roshko structure at very high Reynolds number has been provided by Clemens and Mun-

 0899-8213/91/051193-14$02.00

gal[5] (Fig. 1). The mixing layer seen here was formed between two airstreams at speeds of 430 and 275 m/sec. This composite photo is a schlieren image together with "cuts" through the flow that avoids the spatial integration inherent in shadow–schlieren photos. In this case, a laser sheet was passed through the flow and scattered light from fine alcohol droplets which mark the mixed fluid region. The Brown–Roshko structure and connecting braid regions are visible in the side view, while the two-dimensionality of the structure is seen in the plan view. Also visible is the smaller scale, secondary structure that has been described by Bernal and Roshko.[6] The important point is that the structure seen here is observed at Reynolds numbers, based on local shear layer thickness, velocity difference, and mean kinematic viscosity of 230 000 that is an order of magnitude greater than the studies of Brown and Roshko. Furthermore, the exit of the test section is about 3000 initial boundary-layer momentum thicknesses downstream of the splitter plate. Note also that in Ref. 7 the Brown–Roshko structure was seen to persist to values of the Reynolds number as high as 600 000. When taken together with other studies at lower Reynolds numbers,[8–14] these results are compelling evidence that the large-scale motions are essentially inviscid in nature and exist for all Reynolds numbers beyond some critical value.

The secondary structure seen in Fig. 1 was originally investigated by Bernal and Roshko.[6] They propose that it consists of a series of smaller scale vortices of alternating sign which partially wrap around the primary structure and corrugate the braid region. That the structures are vortices has been verified in the low Reynolds number experiments of Lasheras and Choi,[15] and in high Reynolds number flow by the work of O'Hern.[16] In O'Hern's work, cavitation in the low pressure cores of the streamwise vortices produced a natural flow visualization. Another interesting feature of his configuration is that the shear layer forms between a free stream and a recirculating region behind a vertical plate–not a particularly "clean" flow. Thus the structure appears to be quite robust to external disturbances.

This issue of the robustness of the structures has been the subject of at least two studies which attempted to disrupt them. Breidenthal[17] investigated the influence of the wake of a thick splitter plate as well as that of a significant change in the planform shape, whereby alternate sections of the plate were removed. Wygnanski *et al.*[18] studied the effects of tripping the boundary layer, vortex generators, and high free-stream (grid) turbulence. In every case, the layer is found to recover toward the Brown–Roshko picture, usually after a transition distance where the effects of the disturbance are first felt and then forgotten.

The evidence presented in this section can be summarized as follows. The Brown–Roshko structure in mixing layers is believed to result from inviscid instability and, as such, exists for high Reynolds number flows. Figure 2 (from Coles[19]) is a cartoon (using the terminology of Corcos[20]) of the resulting fluid motion. In a frame of reference moving with the structure, fluid from both free streams is drawn toward the braid region and is sketched as a stagnation region. The outflow from this region then moves toward the cores of the spanwise structures where mixed fluid accumulates. This cartoon will be discussed later in Sec. IV.

B. Jets

While evidence for organization in two-dimensional mixing layers is abundant, the story for jets is much less direct, as will be seen below. However, modern diagnostic and visualization approaches are beginning to reveal the underlying large-scale structures in jets.

The first difficulty is that shadow/schlieren images of jets do not reveal obvious organization as was the case for the mixing layer. This is now believed to be a consequence of the increased complexity of the jet. The experimental evidence suggests that structures in jets are more three dimensional with one structure often partially nested within the other so that laser sheet-cutting techniques are important to finding structure. Additionally, the use of movie sequences and of

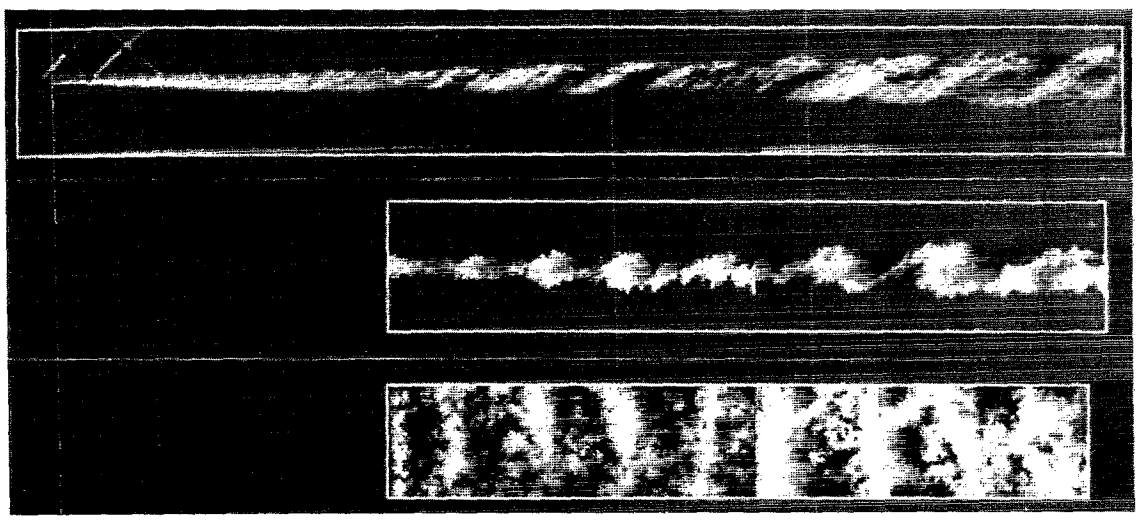

FIG. 1. High Reynolds number shear layer.[5] Top image shows schlieren photographs from $x = 0$–45 cm downstream. Planar side and plan views shown from $x = 15$–45 cm. Re at exit plane = 230 000.

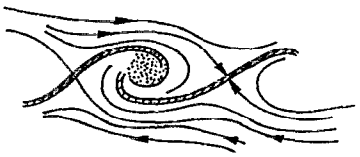

FIG. 2. Cartoon of mean streamlines and molecular mixing zones in the shear layer.[19]

chemical reactions to allow fuel bearing structures to "burn out" and hence become invisible has also proven especially helpful.

Dahm and Dimotakis[21] used a chemical reaction (in water) and a movie sequence to investigate the spatial and temporal evolution of a turbulent jet at a Reynolds number of 10 000. In this case the chemical reactions in their study simulate zero heat release combustion and provide an instantaneous view of the spatial concentration field. At about 150 diameters downstream (their "flame tip") the movie sequences show that the jet fluid reactant is consumed by the reservoir fluid reactant in a quasiperiodic fashion at a frequency that scales with the local large-scale variables. Careful examination of the movie sequence shows that the jet consists of organized structures that convect downstream and burn out quasiperiodically at the tip.

Figure 3 contains results of van Cruyningen *et al.*[22] and shows a planar cut through the centerline of a nonreacting $\mathrm{Re} = 8000$ jet. The structure of the jet is revealed as regions of distinct concentration which decrease in the downstream direction, but in a stepwise fashion, a characteristic first observed by Dahm and Dimotakis[21] (the decrease in discrete steps in Fig. 3 is obscured by the rescaling). It is these large regions of similar concentration that "burn out" quasiperiodically in the study of Dahm and Dimotakis.

To illustrate the jet dynamics in a compact fashion, Mungal *et al.*[23] have used the technique of volume rendering[24] to present many frames of data from a movie sequence simultaneously. Here x-y frames from the movie are stacked sequentially as a function of time, t, to produce a solid object in x-y-t space. A virtual line source of light to the left of the stack provides illumination. Surfaces that would be hidden on the rear face of the stack are removed from view. With this display technique many frames of data can be presented simultaneously, with further examples shown in Ref. 25. In addition, a large-scale structure which convects downstream is revealed as a traveling "bump" in the rendered surface. Figure 4 shows the result of applying the technique to a $\mathrm{Re} = 2\times 10^8$ momentum-driven jet. Several features of the large-scale motion are visible; the structures are seen to grow as they progress downstream, decay in speed, and occasionally pair. This photo establishes the presence of large-scale structure in jets to very high Reynolds numbers, and again

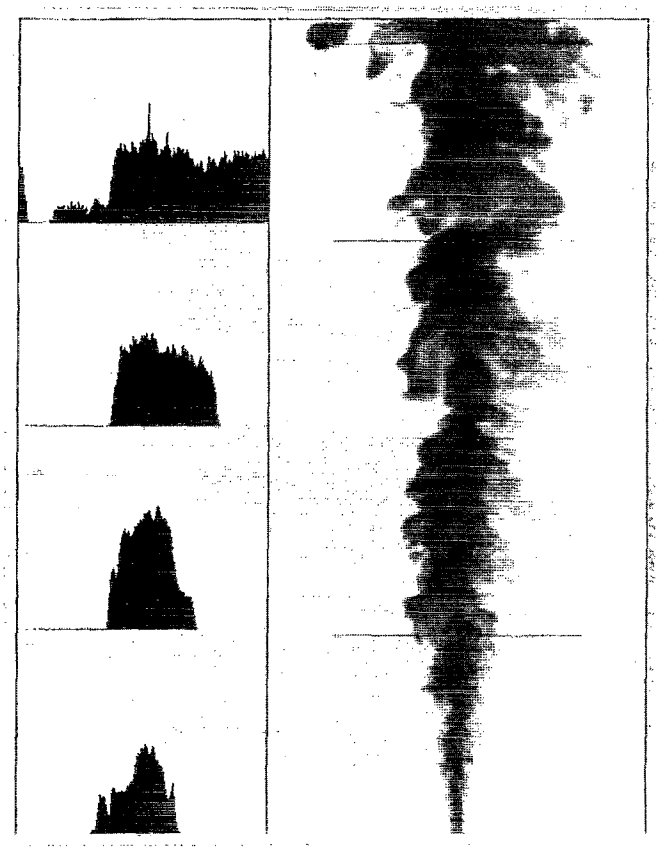

FIG. 3. Planar laser-induced fluorescence cut through the centerline of the $\mathrm{Re} = 8000$ jet.[22] Concentration field rescaled to remove $1/x$ decay. Four instantaneous profiles are shown at the stations indicated.

FIG. 4. An x-y-t volume rendering of the $\mathrm{Re} = 2\times 10^8$ momentum-driven jet.[23] View extends from $x = 400$–2000 ft vertically. Time axis covers $t = 0$–21 sec. Note the presence of organized large-scale structures which convect downstream.

when taken together with previous lower Reynolds number studies,[26–32] suggests that the presence of the large-scale structures is Reynolds number independent.

The organized structure in the round turbulent jet is thus viewed as resulting in motion by which external fluid is entrained and mixed into the main jet body. The entrainment occurs primarily from the upstream boundary of the structures while fluid from deep within the jet is pushed toward the outer jet edges, such motion causing the bumps seen in Fig. 4. Some direct evidence for the large-scale motion is seen in the color photos of Shlien.[33] Here, a thin stream of dye was allowed to enter the jet far field and thus mark the entrained fluid. The dye streamer is seen to enter deep into the jet, cross the centerline, and eventually appear at the outer jet edge, usually within 1 or 2 local jet diameters. Figure 5, from Ref. 34, is a schematic of this type of entrained fluid motion resulting from the large scales. The arrows suggest the type of stirring that results when viewed from the laboratory frame. As can be seen, the recently entrained fluid travels toward the centerline of the jet while the (older) jet fluid is pushed toward the outer edges, and is later reentrained. The instantaneous motion is to be compared with the time-averaged motion seen in Fig. 5(b) which differ from the stirring motions seen instantaneously. This schematic is the analog of that shown for the mixing layer (Fig. 2), and will be used later in Sec. IV.

III. SCALAR MIXING AND CHEMICAL REACTION EXPERIMENTS

Having established in Sec. II that large-scale structures are present in shear layers and jets, we proceed to examine their influence on mixing and chemical reactions in such flows.

A. Shear layers

The first point has to do with the distribution and composition of the fluid that is entrained and mixed in the two-dimensional shear layer. Figure 6, containing results for both gases (Schmidt number, Sc~0.7) and liquids

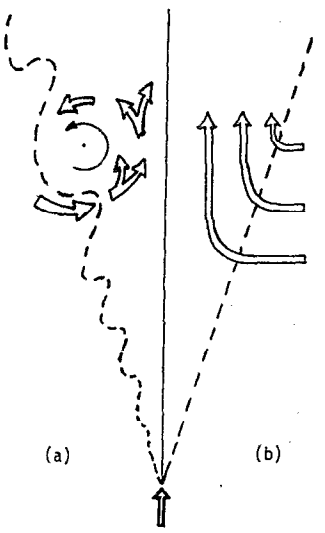

FIG. 5. Schematic of entrained flow into a turbulent jet.[34] (a) Instantaneous flow; (b) time-averaged flow.

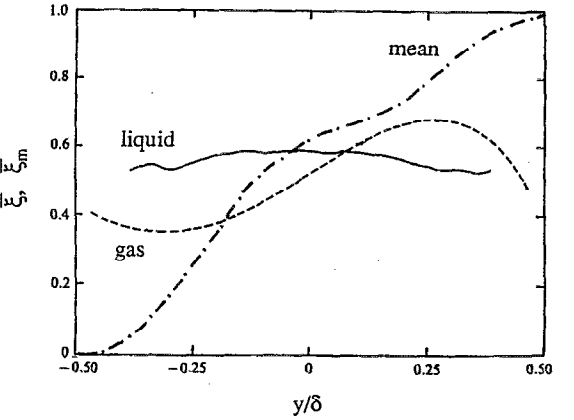

FIG. 6. Mean and mean mixed fluid concentration in the turbulent mixing layer: –·–, mean, liquid,[38] Re = 23 000; ——, mean mixed fluid, liquid,[38] Re = 23 000; ---, mean mixed fluid, gas,[42] Re = 65 000.

(Sc~600), shows the distribution of fluid that is both stirred and mixed, the mean composition, and the distribution of that which is mixed. The mean composition consists therefore of both unmixed free-stream fluid and mixed fluid. In this figure, the mean composition comes from measurements in water but is similar to those observed in gases.

Notice first the striking difference between the mean mixed composition and the mean values. This difference is especially clear for the water experiment where it can be seen that there is virtually no lateral variation in the mixed composition while the mean values follow the S-shaped curve that has been known for many years. Since the (volume) ratio of the high-speed to low-speed fluid mixed in the layer (the entrainment ratio E) is about 1.3 for the present density and speed ratio,[10,35–37] the mixed fluid concentration exceeds one-half.

Next, observe that although the mixed composition in gases also departs markedly from the mean curve, it differs also from the mixed liquid distribution. This is the first indication of what is to be a second theme of this paper, i.e., that the molecular diffusion coefficient influences mixing even at so-called high Reynolds numbers.

Consider next Fig. 7, where four probability density functions (pdf's) of concentration are plotted: (a) for liquids from Koochesfahani and Dimotakis,[38] (b) for gases, from Konrad,[35] (c) a theoretical result from Kollman and Janicka[39] using Reynolds-averaged equations, and (d) the experimental results from Batt.[40] (With respect to theoretical predictions, Batt's results have also been reproduced by the analysis of Pope.[41]) We see that in Figs. 7(a) and 7(b) the peak concentration varies little with the lateral coordinate, again, especially for the liquid experiment. For Fig. 7(c), however, the peak values move as would be expected from the mean curve in Fig. 6. The similar shape of the experimental results of Fig. 7(d) is due to the low resolution of the measuring probe: when the resolution is such that mixed and unmixed fluid cannot be distinguished the shape is consistent with the mean values. The similarity between these latter results is therefore understandable, for when the Navier–Stokes equations are averaged and the diffusion terms

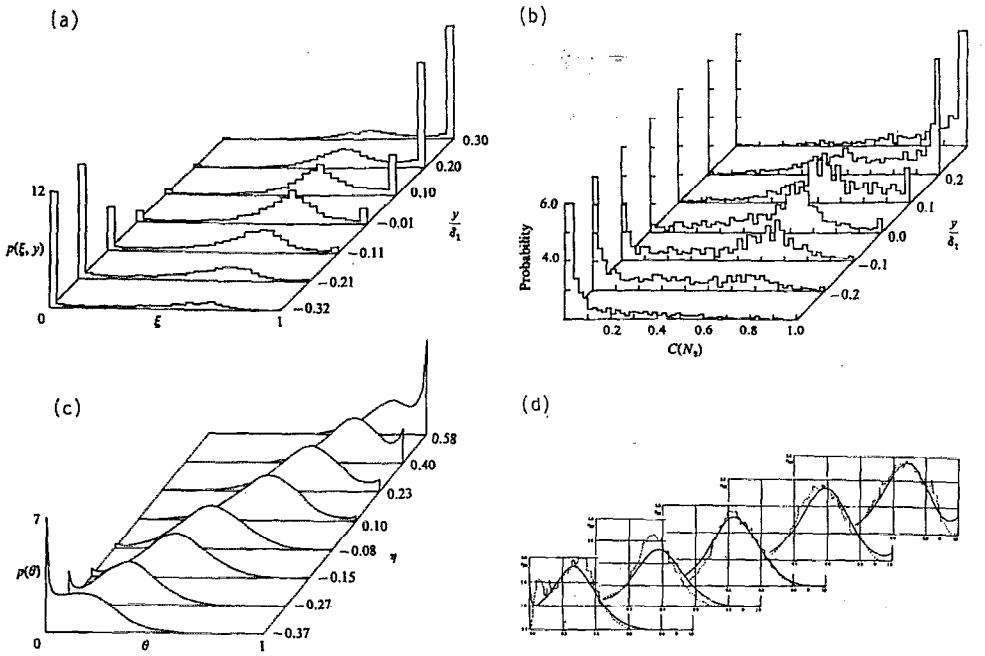

FIG. 7. Probability density function (pdf) of mixture fraction in the turbulent shear layer (a) Koochesfahani and Dimotakis,[38] liquid, Re = 23 000; (b) Konrad,[35] gas, Re = 25 000; (c) Kollman and Janicka,[39] calculations (independent of Sc, Re); (d) comparison of Kollman and Janicka with experimental results of Batt,[40] gas, Re = 80 000.

dropped, again the distinction between mixed and stirred fluid is lost.

The resolution requirements are severe, approaching dimensions the order of the Batchelor scale. In the experiments yielding Fig. 7(a), the liquid pdf, the resolution was approximately the Kolmogorov scale, and hence these results are slightly in error. The effect of resolution limitations is discussed thoroughly in Ref. 38 as is the method for obtaining the results in Fig. 6 that are free from these difficulties. For reasons given later, the gas pdf, Fig. 7(b), is believed to be accurate.

While the emphasis of the present paper is upon mixing, it is clear that one of the primary applications of the ideas is to chemical reactions, and conversely, that much can be learned about mixing from chemical reaction experiments, particularly those in which the reaction cause little, if any, change in the flow. Several such experiments, some associated with the above-mentioned work, are discussed next.

One such investigation involving reactions in water was carried out in the same facility in which the pdf in Fig. 7(a) was measured. For present purposes, the details of the reaction are not important; only the fact that it is fast relative to the mixing rate is required. In this and the following discussions the symbol ϕ denotes the equivalence ratio of a reaction, and means the mass of high-speed fluid required to completely react unit mass of low-speed fluid. Figure 8 shows the distribution of product for two experiments, one with $\phi = 10$ and the other for $\phi = \frac{1}{10}$, such conditions being realized by simply interchanging the fluids of fixed composition from one side to the other. (This has come to be called a flip experiment.) When $\phi = 10$ more product is generated because the "lean" reactant is carried on the high-speed side in this case. The characteristic of the distributions that is emphasized here, however, is their *symmetry*. Although one reactant is almost ten times richer than the other, the product distribution carries little evidence of that fact. It is the nearly flat mixed fluid composition in Fig. 6 that is the source of the symmetry.

Consider next a similar experiment at about the same Reynolds number in gases.[42] The results are shown in Fig. 9, where the flip is made for a range of ϕ's. Here the nitrogen stream carried dilute concentrations of hydrogen and fluorine and traces of nitric oxide sufficient for the reactions to be fast, i.e., mixing limited. The time mean temperature was determined from time traces at eight stations across the layer. Focusing on $\phi = 8$ and $\frac{1}{8}$ we see again higher temperature (or more product) for $\phi = 8$ and that in this case the profiles are not quite symmetric albeit the deviation is small, in accordance with the small slope of mean mixed composition in gases plotted in Fig. 6.

As was mentioned, the mean temperature profiles in Fig. 9 came from temperature–time traces taken at eight stations across the shear layer, Fig. 10 being an example for $\phi = 1$. These traces provide a clear explanation for the differ-

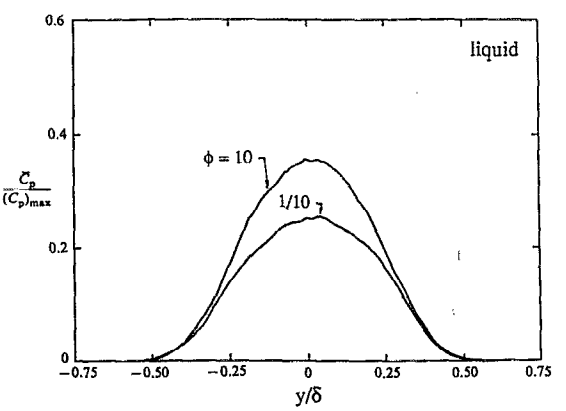

FIG. 8. Mean product profiles for fast chemical reaction in liquid.[38] $\phi = 10$ and $\frac{1}{10}$ from top to bottom; Re = 23 000.

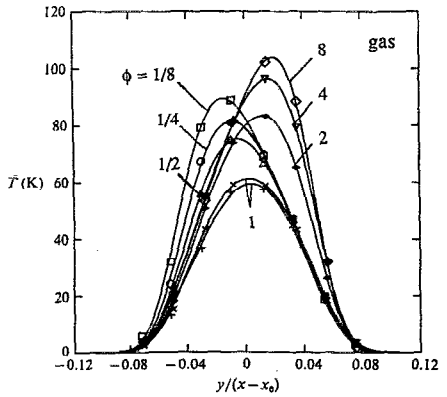

FIG. 9. Mean temperature (product) profiles for fast chemical reaction in gases.[42] Left curves $\phi = \frac{1}{8}, \frac{1}{4}, \frac{1}{2}, 1$ from top to bottom. Right curves $\phi = 8, 4, 2, 1$ from top to bottom; Re = 65 000.

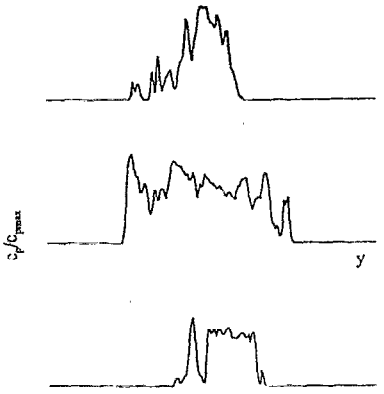

FIG. 11. Instantaneous product profiles in a reacting, liquid mixing layer, and as a function of lateral coordinate, Re = 23 000, from Koochesfahani (unpublished).

ence in the mean and the mean mixed profiles that has been emphasized in the preceding discussion. Observe that the maximum temperature is of similar magnitude at the eight stations indicating that the mixed composition likewise, is nearly the same. The approximately Gaussian shape in Fig. 9 arises from the relative times that the various probes spend in mixed and unmixed fluid. Similar concentration–time traces from both passive and chemical reaction experiments in the water shear layer experiment (Ref. 38) exhibit the same characteristics and lead to the same conclusions concerning the mean concentration distribution in Fig. 8.

When the Konrad pdf, Fig. 7(b), is used to compute the mean temperature for the hydrogen–fluorine experiment, the results are in good agreement with those shown in Fig. 9 for $\phi = 8, 1, \frac{1}{8}$ (Mungal, unpublished). (A different conclusion drawn in Ref. 42 arose from the use of a nominal layer width for normalizing y, the lateral coordinate. This now seems improper in view of the large variation in layer widths that have since been observed.) It is this computation that establishes the accuracy of this pdf.

Next of interest are several (unpublished) instantaneous product profiles (Fig. 11) for the liquid experiment kindly furnished to the authors by M. Koochesfahani. The shapes of these profiles are to be contrasted with the mean values plotted in Fig. 8. What is to be noted particularly, are the remarkably steep sides and large interior fluctuations in these shapes. The significance of these features will be discussed in Sec. IV after additional profiles, such as those in Fig. 3, have been presented for jets.

When the product concentrations and temperature profiles in Figs. 8 and 9 are integrated and normalized to obtain total reaction product amounts that can be compared, it is found that about twice as much product is generated in the gas flow as in the liquid—the results are given in Sec. IV, where the significance of the difference is discussed.

It is instructive to examine next the effect on the mean temperature profiles of another parameter, the Damköhler number (Da), defined here as the ratio of the flow time to the measuring station to the chemical reaction time. Figure 12, from Ref. 43, shows the result for $\phi = \frac{1}{8}$ in gases where it is noted that as the reaction rate coefficient is reduced from that yielding mixing limited conditions to slow values, not only does the amount of product drop, but the profiles become symmetric (becomes liquidlike as we say). Recall that the liquid reaction product profiles are symmetric, but that the gas is not. The similarity of the effects of such unrelated

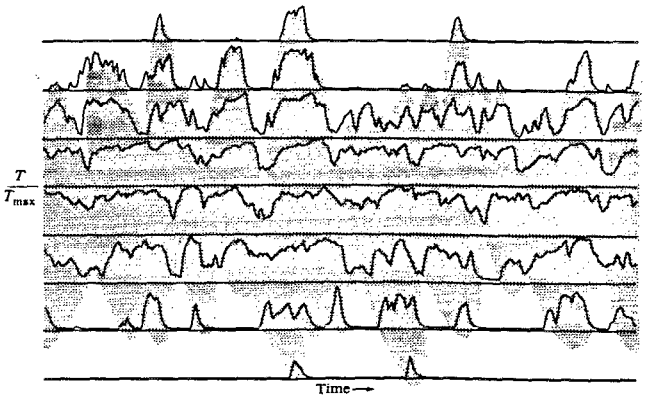

FIG. 10. Temperature–time traces measured simultaneously at eight transverse locations for fast chemical reaction in gases.[42] High speed on top. Time axis = 51.2 msec. $\phi = 1$, Re = 65 000.

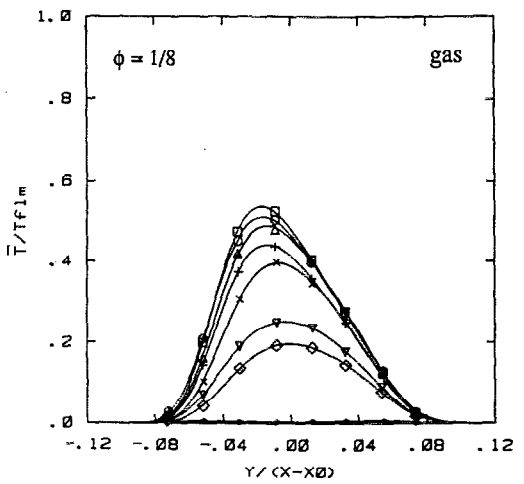

FIG. 12. Mean temperature (product) profiles for variable reaction rate in gases.[43] $\phi = \frac{1}{8}$ for all cases. Reaction rate decreases from top to bottom; Re = 65 000.

parameters (Sc, Da) provides, we believe, an important clue to the nature of stirring and mixing in the turbulent shear layer. An explanation for the similarity is offered in Sec. IV.

B. Jets

We take up next results from turbulent jets, both axisymmetric and two dimensional, where, in contrast to the shear layer, a finite flux of one fluid, the jet flux, mixes with an (effectively) infinite extent of reservoir fluid. This difference provides data with a different set of clues concerning the nature of stirring and mixing in turbulent shear flows.

The first of these clues is in the results of an experiment carried out in the 1940s by Hottel[44] and co-workers at MIT. There, Weddell studied jets consisting of an alkali solution marked with phenophthalein discharging into an acid reservoir. The jet, which is initially red, becomes colorless when it entrains and mixes with sufficient acid. Dahm *et al.*[21,45] have repeated this experiment using fluorescence of the jet fluid as the pH indicator. In the experiments, the reservoir–jet normality ratio, or ϕ, is the mass of reservoir fluid required to cause the color or fluorescence to vanish from a unit mass of jet fluid when the two are mixed homogeneously. These investigators studied the "flame length" dependence on Reynolds number and on ϕ, where flame length means the distance for the color or fluorescence to disappear. At the flame end, *every* element of jet fluid is mixed with at least ϕ parts of reservoir fluid.

Their results, from Ref. 45, are collected in Figs. 13 and 14 and constitute two remarkable findings. First, beyond Re$\sim$3000 the mean flame length becomes independent of the Reynolds number, and second, this length varies linearly with ϕ.

It is established by dimensional reasoning and experiment that the mass flux of a jet rises linearly with the axial distance,[46] and, consistently, the mean concentration falls like $1/x$. The Weddell–Dahm experiment provides information about the rate of molecular mixing. In particular, it shows that *every element* of jet fluid is mixed with at least ϕ parts of reservoir fluid at the location $x = 10\phi$ (Fig. 14); i.e., that the highest concentrations of jet fluid also fall like $1/x$. Evidence that this same conclusion holds for gaseous flames (when jet diameter d is properly redefined) is discussed in Dahm[47] and in the jet model of Broadwell.[48] This conclusion, suggesting that the mixed concentration *on the jet centerline*, where the concentration is highest, is independent of both Schmidt number and Reynolds number, has been confirmed by the recent highly resolved concentration measurements of Dowling and Dimotakis[49] in a gas jet discharging into a reservoir of equal density. Figure 15 shows the resulting pdf's together with those of other investigators. We speculate that the solid symbols represent data influenced by buoyancy and are thus ignored here. To repeat, the data of Fig. 15 is evidence that neither Reynolds nor Schmidt numbers influence the composition of fluid on the jet centerline. This remarkable result, in apparent contradiction with those for the shear layer, is discussed further in Sec. IV.

The preceding discussions have dealt with the mean flame length and its implications for the mean molecular mixing rate. An important discovery of Dahm and Dimotakis was the large-scale fluctuation in this quantity. It is, of course, the intrinsic nature of turbulent flows to exhibit fluctuations, but what was discovered in these experiments was an almost periodic, nearly constant, large fluctuation. The data, showing that the length fluctuations scale with the local jet diameter δ and the frequency with u/δ (where u is the

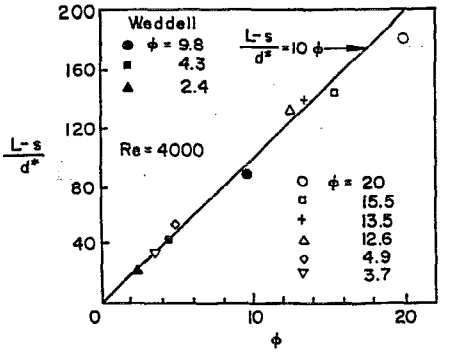

FIG. 14. Mean turbulent flame length at high Reynolds number versus equivalence ratio.[45]

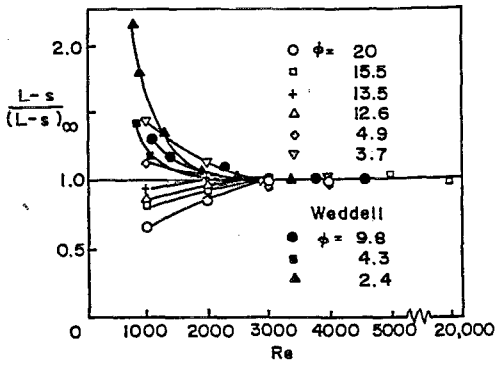

FIG. 13. Mean turbulent flame length normalized by its asymptotic value versus Reynolds number and equivalence ratio.[45]

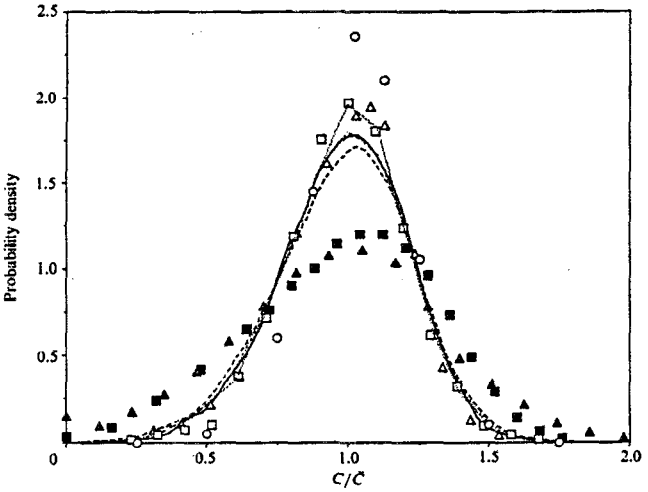

FIG. 15. Probability density function (pdf) of mixture fraction along the jet centerline.[49] ——, Re = 5000; ---, Re = 16 000;–·–, Re = 40 000.

local mean centerline velocity), appears in Refs. 21 and 47.

Mungal and O'Neil[50] and Mungal *et al.*[51] followed up the above work by performing similar experiments to those of Dahm but using burning (gaseous) systems. Volume rendering shows the orderly progression of burning large-scale structures up through the jet body which burn out quasiperiodically at the flame tip.[51] To first order the appearance of the liquid and gaseous flame are found to be remarkably similar.

The shear layer section began with a discussion of the lateral concentration profiles; this section takes up the nature of such profiles in jets. Corresponding to Fig. 6 is Fig. 16 for jets from the study of Papantoniou and List[52] (similar findings were reported earlier by Dahm[47]). Here, although the difference is not as striking as in Fig. 6, the mean mixed concentration departs significantly from the mean value near the edges of the jet. (References 52 and 27 show that for buoyant jets and jets in coflow the departure is larger.)

Several instantaneous profiles from Refs. 22, 47, and 52 appear in Figs. 3 and 17. Similar shapes have been observed by Dibble *et al.*[53] Perhaps the first of such observations is that of Uberoi and Singh[54] from their study of the temperature distribution in a slightly heated two-dimensional jet. Note the similarity between these instantaneous profiles and those in Fig. 11 for the shear layer. The significant common features of the instantaneous profiles are the large fluctuations about nearly constant values and the sharp drop at the edges. Such features in various cumulus cloud profiles, such as droplet density, are reported in Ref. 55. See Figs. 1(a) and 8(b) of this work and the accompanying discussion.

A difference between the shear layer and the axisymmetric jet profiles is the occasional presence of two mixed fluid concentration levels in the latter case. A possible explanation for this difference, mentioned in Sec. II, was proposed in Ref. 21, where it was pointed out that two structures of different compositions are often nested.

It is relevant at this point to discuss a result from the study of Antonia *et al.*[56] of a heated two-dimensional jet. Figure 18 contains temperature and velocity time traces at $x/d = 40$ and at the velocity half-width lateral station. The numbers in parentheses denote locations along the span of the jet. The simultaneity of the temperature fronts, marked by the arrows, indicates the nearly two-dimensional nature of the structures. The temperature ramps, the sharp rise followed by a gradual decline, have also been observed in axisymmetric jets by many others including Gibson *et al.*,[57] Dowling,[58] van Cruyningen,[59] Antonia *et al.*,[27] and in water by Dahm.[47] In shear layers they have been noticed and analyzed by Fiedler,[10] Konrad,[35] Mungal and Dimotakis,[42] and Mungal and Frieler.[43] In boundary layers, ramps have been reported by Chen and Blackwelder.[60] Intriguingly, such temperature and humidity ramps have been reported in the atmospheric boundary layer, where, of course, the Reynolds number is very high: Van Atta estimates values of Re_λ of the order of 5×10^3. See Refs. 61 and 62, for instance, for a discussion of these observations.

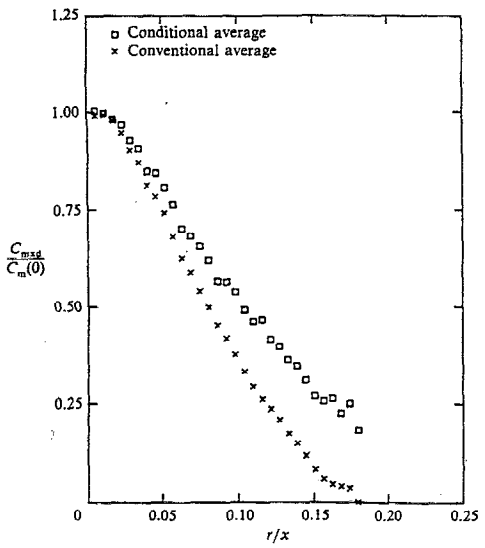

FIG. 16. Radial profile of mean and mean mixed concentration in a turbulent jet.[52]

IV. MODELS

This section provides a fairly extensive discussion of two models and brief remarks about several other modeling approaches.

A. A two-stage Lagrangian model

The early experiments on shear layers and jets at high Reynolds numbers that revealed large-scale structures, together with results from the Weddell flame simulation in water, suggested a simple model[63] of mixing and chemical reactions in these flows. The model, as subsequently modified and extended,[64] is described next. As will be seen, it provides a framework for interpreting the above discussed observations.

It is easier for present purposes to restrict attention to cases for which the Schmidt number is $Sc \geqslant 1$ and to start with the shear layer. The model is based upon a Lagrangian picture of the flow in which the large-scale unsteadiness is an essential feature and in which discrete quantities of free-stream fluids enter the layer at large scale (Roshko's gulping[2]). These streams flow into the braids, Fig. 2, begin to intertwine, and enter the spanwise structures. During this time, the interface is stretched at an ever increasing rate until the motions reach the Kolmogorov viscous scale $\lambda_k \sim \delta/\mathrm{Re}^{3/4}$, where δ is the local width and $\mathrm{Re} = \delta \Delta u/\nu$ the local Reynolds number. The time for this inviscid "cascade" scales with $\delta/\Delta u$ and initially the interface is subjected to the large-scale strain $\Delta u/\delta$. At this initial condition, the viscous layer thickness is the Taylor scale, $\lambda_t \sim \delta/\mathrm{Re}^{1/2}$ and the embedded scalar thickness is $\delta/(\mathrm{Re}\,\mathrm{Sc})^{1/2} = \delta/\mathrm{Pe}^{1/2}$, where Pe is the Péclet number. Batchelor[65] shows that the local straining reduces λ_k to $\delta/(\mathrm{Re}^{3/4}\,\mathrm{Sc}^{1/2})$ in a time $(\delta/\Delta u)(1/\mathrm{Re}^{1/2})$ ln Sc. Then, since the time for scalar diffusion across this reduced (Batchelor) scale is only $(\delta/\Delta u)/\mathrm{Re}^{1/2}$, when $\mathrm{Re}^{1/2} \gg \ln \mathrm{Sc}$, this scalar diffusion time is negligible compared to $\delta/\Delta u$, the cascade time. This argument leads to the simplifying assumption that the inter-

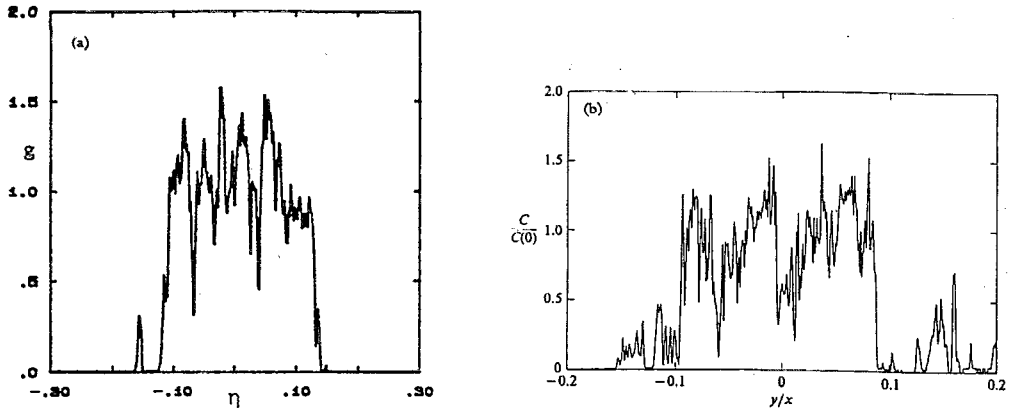

FIG. 17. Instantaneous concentration profiles in a turbulent jet. (a) Dahm and Dimotakis,[21] Re = 5000, $x/d = 300$; (b) Papantoniou and List,[52] Re = 5600, $x/d = 150$. Note the similarity to Fig. 3.

twined fluids mix instantaneously when the scale λ_k is reached.

Next we make use of the intuitive notion that the interfacial area per unit volume grows slowly at first, then with increasing rapidity as λ_k is approached. (Some support for this idea is found in chaotic advection studies where even for two-dimensional motions such interfaces grow exponentially.) Combination of this picture with the above discussion of the diffusion time suggests the following simplifying approximation. The diffusion layer thickness is λ_t for the time $\delta/\Delta u$ after which the entangled fluids mix instantaneously. As fluids continue to enter the layer farther downstream, the process repeats.

The same description is taken to apply to the jet (Fig. 5), where now the Taylor layers form between the entering reservoir fluid and the jet plus reservoir fluid mixture, the composition of which changes with downstream distance.

In both flows, the above-mentioned events take place at random times and locations; the model is intended to describe the averaged consequences of such events. Taking S to be the average surface area per unit volume at the large scale, equal to B/δ, with B a constant, we find that the contribution resulting from the Taylor layers to the mixed volume per unit volume of the layer is

$$\lambda_t \cdot S = \frac{\delta}{(\mathrm{Re\,Sc})^{1/2}} \cdot \frac{B}{\delta} = \frac{B}{(\mathrm{Re\,Sc})^{1/2}}.$$

At any axial station then the molecularly mixed fluid volume fraction V_m can be written

$$V_m = A + B/(\mathrm{Re\,Sc})^{1/2}$$

in which A is the average mixed volume fraction generated when the entrained fluid reaches λ_k. The constants A and B are determined from experiments as described later.

In the application of these ideas, the mixture formed instantaneously at λ_k is taken, as a further simplification, to be at a single composition and is hence called the homogeneous mixture. In both the shear layer and the jet, the continual stirring by the large-scale motions makes a more complex treatment of doubtful value. This stirring also implies that it would be difficult to justify any other than a one-dimensional assumption for the mixed fluid composition. Figure 6, of course, helps justify this approximation. The averaged flows as described above can be represented schematically as in Fig. 19.

In the models, the mean fluid motions are taken from standard similarity laws with their empirically determined constants.

In Ref. 64, this analysis is applied to a low-speed shear layer between two nitrogen streams, one carrying hydrogen and the other fluorine, both in dilute concentrations. Flux equations are derived for the reactants in the two mixed streams. They show that when $x/\bar{u}$ is replaced by time in the homogeneous mixture equations, these equations describe exactly the fluorine and hydrogen equations in a perfectly stirred reactor to which the Taylor streams are steadily added. It is helpful, therefore, to represent the flows as in Fig. 19. In this study, the Taylor layers are represented as stagnation point flows formed between the two free streams and treated by a boundary-layer integral analysis. At this level of approximation, the result is again a set of equations for a perfectly stirred reactor. These approximations combined with

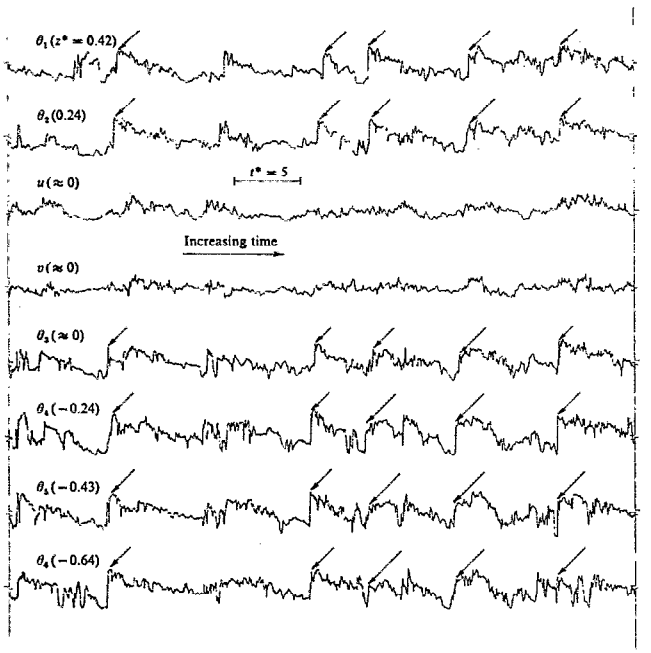

FIG. 18. Time traces of temperature and velocity fluctuations obtained with a spanwise rake of cold wires in a turbulent plane jet.[56]

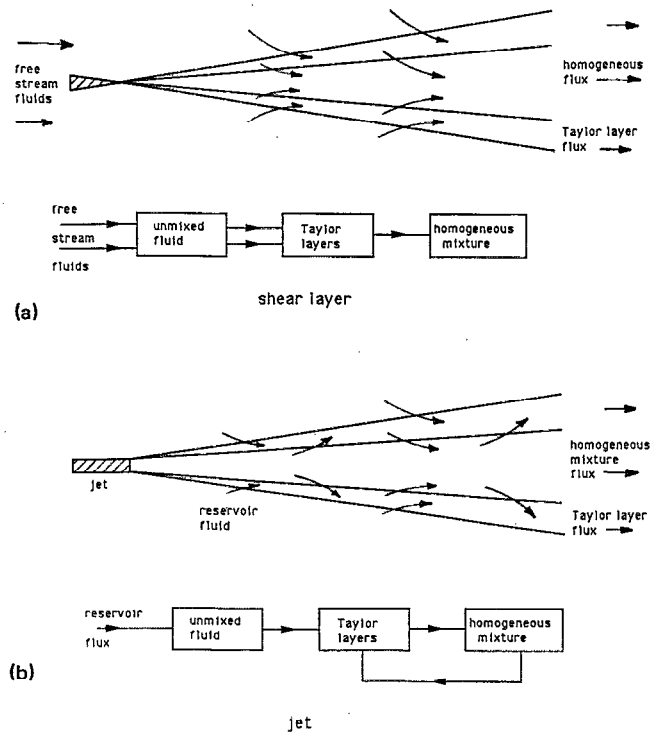

FIG. 19. Sketch of mixed fluid flux and the model schematic for (a) shear layer and (b) jet.

the simplification of the hydrogen–fluorine chemical kinetics allowed an analytical treatment of the problem. The analysis was applied to four sets of experiments, Refs. 38 (liquid), 42 (gas), 43 (Da effect), and 4 (Re effect), as described next.

In the chemical reaction experiments the amount of product was characterized by the "product thickness" defined by

$$\delta_P = \int_{-\infty}^{\infty} \frac{c_p(y)}{c_\infty}\, dy$$

where c_p is the molar product concentration and c_∞ is the fluorine concentration in the low-speed stream. The equivalence ratio ϕ is the ratio of the free-stream fluorine concentration to that of the hydrogen. Figure 20 shows the dependence of δ_P, normalized by the layer thickness, on ϕ for both the H_2–F_2 reaction and a reaction in water where ϕ is equivalently defined. In both experiments conditions are such that the reactions are fast enough to cause them to be mixing limited. The two solid symbols are experimental points from which the constants A and B were determined. Observe first as noted above that approximately twice as much product comes from the gas reaction as from that in water.

The form of the plot illustrates the nature of the model. In water, the Sc = 600 results, where the contribution to δ_P from the Taylor layers is negligible, the amount of product rises with increasing high-speed concentration at fixed concentration in the low-speed stream, i.e., with $1/\phi$ to the value $1/E$ at which condition all the low-speed reactant has been converted to product. (Recall that E is the entrainment ratio.) The dashed line for gases comes from adding at each ϕ the Taylor layer product to that of the homogeneous mixture.

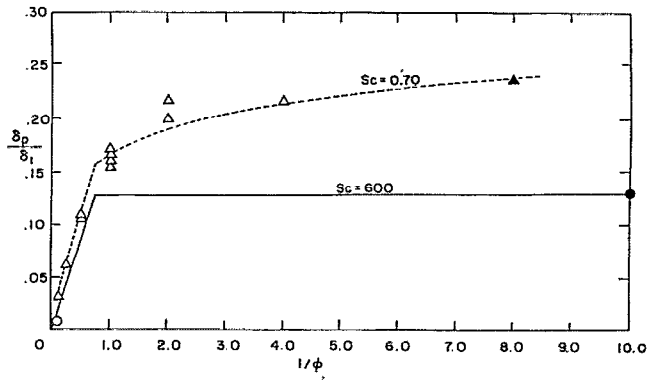

FIG. 20. Normalized product versus equivalence ratio showing model predictions for gases and liquids.[64] Triangles correspond to data of Fig. 9, circles to data of Fig. 8.

As is described in Ref. 43, the overall reaction rate of the H_2–F_2 reaction could be varied by adjustment of the trace nitric oxide concentration required to initiate the reaction. In this way a Damköhler number, $\mathrm{Da} = k(c_H)_\infty x/\bar{u}$, that arises in the analysis could be varied from zero to the mixing limited conditions. Here k is the global reaction rate coefficient, $(c_H)_\infty$, is the hydrogen free-stream concentration, x is the distance to the measuring station from the location of the mixing transition, and $\bar{u}$ is the mean speed. Figure 21 shows the results with the contributions from the Taylor layers [here marked $(\delta_P)_f$] and the homogeneous zone [here marked $(\delta_P)_h$] indicated separately.

It is useful next to discuss the effects of the Reynolds number since when Re is changed by changing the velocities, as was done in the experiments,[4] there is an accompanying change in the Damköhler number. Figure 22 compares the theoretical results for gases with several reaction rates to the experimental values of Ref. 4 mentioned above (denoted by circles). The solid symbols mark the same conditions as in Fig. 20 and the curve $k/k^* = 1$ is to be compared to the

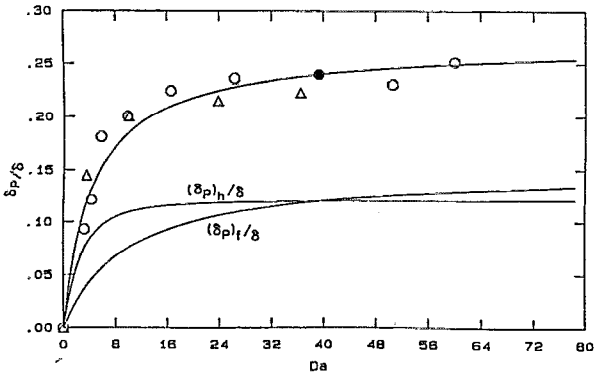

FIG. 21. Normalized product versus Damköhler number, compared to experimental results.[64] Lower lines show contributions to total from homogeneous mixture (h) and Taylor layers (f). Circles, Re = 65 000; triangles, Re = 130 000.

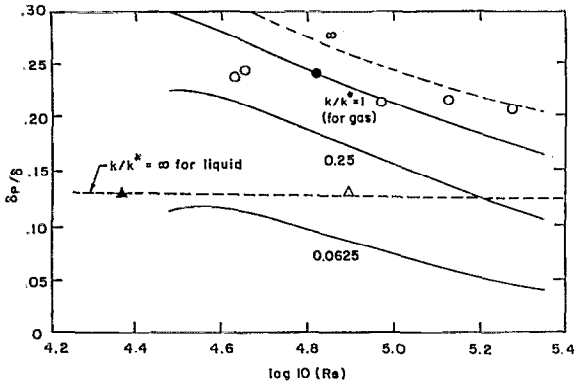

FIG. 22. Normalized product thickness versus Reynolds number.[64] Circles are experimental results in gas. Triangles are results in water. Dashed lines for infinite reaction rates. Solid lines for finite reaction rate.

experimental H_2–F_2 values. The agreement is only qualitative. For the liquid reaction, however, the agreement is good.

The curves for the infinite reaction rate illustrate the effect of Reynolds numbers alone, showing the gas value asymptoting to that of the liquid as $\mathrm{Re}\to\infty$. It is instructive at this point to sketch the model behavior as it approaches this limit. It is clear that at any fixed, finite Reynolds number, the product thickness can be reduced arbitrarily by increasing the Schmidt number. Thus we speculate that the behavior is as sketched in Fig. 23. The finite value for δ_P/δ for $\mathrm{Re}\to\infty$ would seem, intuitively, to imply that the interface becomes a volume filling surface at this condition. A finite flame length for a jet, for fixed ϕ as $\mathrm{Re}\to\infty$, implied by Fig. 23 leads to a similar conclusion. [In the sketch, the curves below the asymptotic value are outside the range of the model as presently formulated: they do not meet the condition $\mathrm{Re}\gg(\ln \mathrm{Sc})^2$.] We note at this point that Dimotakis[66] has formulated a model for this flow which, agreeing similarly with the H_2–F_2 and water reaction data discussed above, yields the limit $\delta_P/\delta = 0$ for $\mathrm{Re}\to\infty$ at fixed Schmidt number.

In Refs. 63 and 64 the Taylor layers were also referred to as flame sheets, a nomenclature that has proved confusing. In the combustion literature, the latter term refers to the zone within which chemical reactions take place and for fast reactions would be a thin sheet occupying only a small fraction of the diffusion zone (the Taylor layer). Of course, if only mixing and not chemical reactions are under discussion, the term flame sheet would be entirely inappropriate. Next it is interesting to note that in Ref. 67 Saffman wrote, "As is well known, viscous effects in motions at large Reynolds numbers are confined in laminar flows to boundary layers and vortex sheets whose thickness is proportional to the $\frac{1}{2}$ power of the viscosity. It is a mystery why turbulence has $\nu^{3/4}$ rather than $\nu^{1/2}$ dependence for the length scale of the viscous effects." The picture of the flow on which the present model is based implies that viscous effects would be felt at the $\nu^{1/2}$ scale as well as the smaller scales generated by the interface stretching.

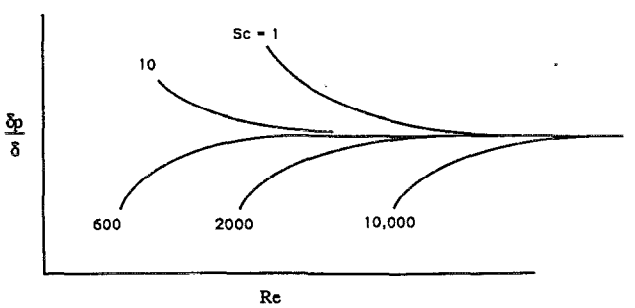

FIG. 23. Model prediction of limiting normalized product as a function of Sc and Re for the shear layer.

Several matters left unexplained in Sec. III are taken up next, the first being the similarity of the effects on product profiles in the shear layer of changes in the Schmidt number and Damköhler numbers. The ideas underlying the model provide a straightforward explanation. When the diffusion coefficient is low ($\mathrm{Sc}\gg 1$) there is negligible reaction in the Taylor layers, hence a delay after the reactants enter the shear layer before product is generated, and hence a symmetric profile. A reaction rate reduction has the same consequences. There is even crude quantitative support for this argument. Recall that in the gas experiment approximately one-half the reaction products lie in the Taylor layers and note that the temperature profiles become symmetric when the average temperature is reduced by about one-half.

Another point has to do with the independence of the jet centerline pdf from the Schmidt and Reynolds numbers in contrast to the shear layer mixing dependence on these parameters. Other observations from the Dowling and Dimotakis[49] jet study provide a plausible explanation. They find no pure (unmixed) reservoir fluid on or within a few degrees of the centerline but toward the jet edge, of course, a rising amount. Furthermore, although the data are sparse, the pdf in this region does depend on both the Schmidt and Reynolds numbers and in a way consistent with the thinning of the Taylor layers there as these parameters increase. All these results are consistent with the idea that the jet "core" constitutes the "homogeneous" mixture of the model while the outer regions consist of both this mixture and the Taylor layers.

Note also that the picture of successive cascades to a Kolmogorov scale in the jet, in a distance that scales with the jet diameter at which the cascade begins, explains both the dependence of the pdf on x/d and the large-scale fluctuations in flame length.

The simplicity of the model is sufficient to permit treatment of complete chemical kinetic system even for such reactants as methane–air where as many as 250 reactions may be involved. Since the study of the pollutant formation in many fuel–air systems may require the use of such complete chemical systems, the jet model, Ref. 48, is particularly suited for this application. Reference 68 describes an initial step in a continuing program of such studies. On the other hand, the ideas on which the model is based allow a simple treatment of flame blowout of jets[69] and jets in coflow,[70] in which the chemistry is highly simplified.

Another application of the shear layer model in which

the complete chemical kinetics set needs to be considered is the hydrogen–air reaction in supersonic flow (Miller *et al.*[71]). A noteworthy feature of this study is the critical effect of the reaction in the Taylor layers on the time or distance required for completion of the reaction.

Other models having some elements in common with the above-described approach include that of Dimotakis[66] mentioned above, but one in particular, that of Effelsberg and Peters,[72] has considerable similarity. They, in examining the data of LaRue and Libby[73] for the wake of a heated cylinder, find that the temperature pdf measured at each transverse location can be divided into three parts (1) unmixed fluid, (2) internal "superlayer," and (3) fully mixed fluid. Making a best fit to data with these three components, they also find a mixed fluid contribution with a peak that does not vary with the transverse coordinate. A difference from the above-described model is that the scale of the superlayer is identified with the Kolmogorov scale instead of the Taylor scale.

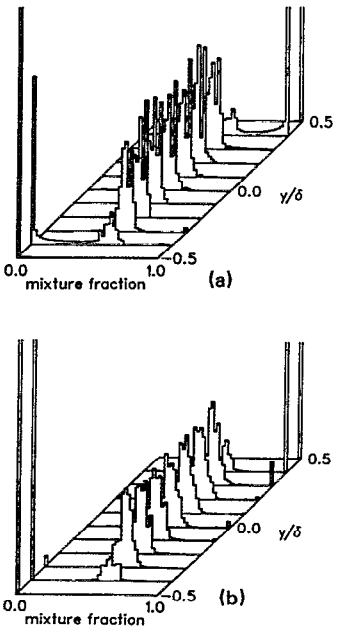

FIG. 24. Probability density function of mixture fraction versus transverse distance as predicted by the linear eddy model.[75] (a) Gas (Sc = 0.7), Re = 10 000. (b) Liquid (Sc = 600) Re = 10 000.

B. The linear eddy model

Another original and intriguing way of incorporating the large-scale motions into a model of scalar mixing in turbulent flows is described in a series of papers by Kerstein. The procedure, called the linear eddy model, has been applied to scalar mixing in homogeneous turbulence,[74] the planar shear layer,[75] homogeneous round jets,[76] and inhomogeneous round jets.[77] While the basic concepts underlying the model are the same in these cases, one of the strengths of the model, the brief discussion here will be confined to the shear layer. To quote from Ref. 75: "The linear eddy modeling approach involves the representation of a spatially developing flow by a simulation of the time development along a transverse line moving with the mean flow. Scalar quantities evolve by Fickian (molecular) diffusion and by randomly occurring spatial rearrangements, representing turbulent convection." Thus, in the language of the Symposium, stirring is simulated by the spatial rearrangements and mixing by the exact computation of molecular diffusion subsequent to the rearrangement. The model thus deals explicitly with the effects of Reynolds and Schmidt numbers and can also treat various Damköhler numbers.

Results from varying only the first two parameters are reproduced here from Ref. 75. Figure 24 shows the spatially resolved pdf of the concentration field in the shear layer for gases and liquids at two Reynolds numbers. Comparison of Figs. 24 and 7 indicate that the model correctly reproduces both the invariance of the peak concentrations with y/δ in both gases and liquids as well as the (Reynolds number dependent) wings in gases and their absence in liquids. Significantly, when the spatial rearrangements are only small scale, the peak of the pdf is found to vary with y/δ.

Figure 25 shows the agreement between the model results and the experimentally observed dependence of the product thickness on the Schmidt and Reynolds numbers. There is also an extensive discussion of the Damköhler number influence and of its correct formulation. In summary, this new approach to the analysis of scalar mixing and chemical reaction shows considerable promise of yielding new insight into these processes.

V. SPECULATIONS ABOUT SHEAR FLOW MIXING AND CHAOTIC ADVECTION

This section contains some tentative thoughts about the connections between the concepts of chaotic advection and turbulent shear flow mixing. For extensive discussions of the subject see for instance, the papers (and their references) of Aref,[78] Ottino,[79] Leonard *et al.*,[80] and the editors' discussion of Ref. 81. Here we wish only to draw attention to the similarity of the scalar fields observed by Dahm and Buch[82] in a coflowing jet to those generated by Leong and Ottino[83] in a closed chaotic flow apparatus, and to comment on the study of Aref and Jones.[1]

This latter study, concerning the separation of particles by chaotic advection, seems relevant to the subject of the mixing transition in the shear layer and perhaps to shear flows in general. Aref and Jones investigate by computation

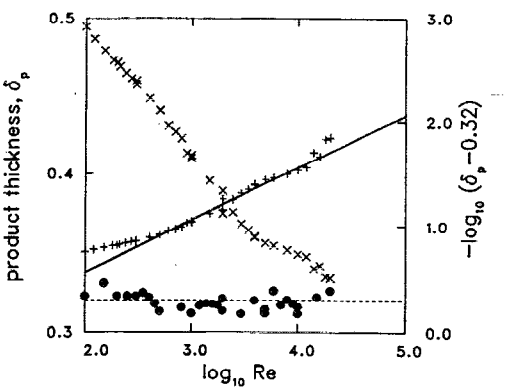

FIG. 25. Product thickness versus Re for gas (×) and liquid (●), from the linear eddy model.[75] Gas results replotted (+) as the difference between gas and liquid. A solid line slope of $\frac{1}{2}$ is shown for comparison.

a scheme for separating particles, but the results can be used to infer some of the characteristics of mixing in such flows. They examine the configuration shown in Fig. 26 in which the dark spot marks the initial location of a set of diffusing particles. The cylinders are rotated so as to cause Stokes flow in the background fluid in which the particles diffuse. After prescribed rotation schedules, one steady, the other unsteady, the motion is reversed and the background fluid returned to its initial state. The focus of the paper is upon the large difference in the degree of return of the diffusing particles to their initial state in the two cases, the steady flow causing integrable advection and the unsteady, chaotic advection.

We identify a fall in the percent return with enhanced mixing and look at only two cases, Figs. 27(a) and 27(b) [Figs. 2(b) and 2(d) of the original paper]. For the smallest diffusivity, there is little mixing in the integrable case, but for chaotic advection, a steep rise follows the initially flat region. At the highest diffusivity, the mixing begins immediately and there is almost no difference in the two cases.

The relationships that we see in the above work to the mixing transition in the two-dimensional shear layer may be summarized as follows.

First, in the shear layer, the sudden rise in the degree of mixing at the transition[17,35] takes place in a small number of pairings, perhaps one or two. This is observed in both experiments[84] and in direct numerical simulations.[85] In the Aref–Jones work, the fall in the degree of return occurs after only a few cycles, and, for small diffusivity, is also abrupt.

In the shear layer, the increase in mixedness at the transition is large for small diffusivity, as in water, but much smaller when diffusivity is large, as in air. A similar effect is seen in comparing Figs. 27(a) and 27(b). Here, for small diffusivity the difference in the return between integrable and nonintegrable motion is large, but negligible when diffusivity is sufficiently large. In other words, in air the diffusion coefficient is large enough to cause considerable mixedness even before the chaotic motion arises, but for water, this motion is needed to produce the asymptotic degree of mixing.

Another relationship between the two flows is suggested by the Aref–Jones correlation of their numerical data. They find that the number of cycles to reach the steep fall-off can be scaled by equating the striation thickness generated by the chaotic motion to the diffusion thickness. We speculate that the mixing transition takes place when the chaotic motion leads to a state where the Taylor layers begin to overlap.

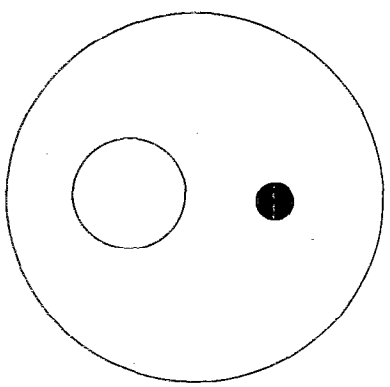

FIG. 26. Definition sketch for numerical stirring experiments of Aref and Jones.[1] Two-cylinder geometry is shown. The black dot represents the initial location of advected particles.

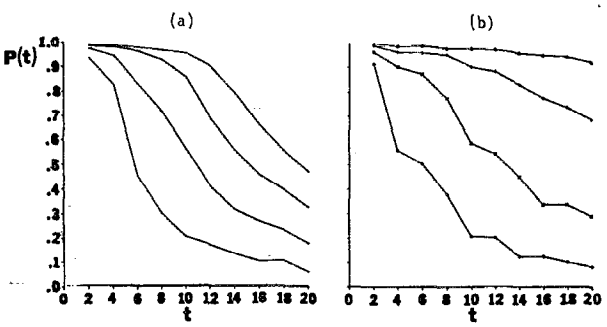

FIG. 27. Graphs of return percentage $P(t)$ versus stirring time t for decreasing diffusivity (bottom to top): (a) Chaotic advection, (b) integrable advection; from Aref and Jones.[1]

These possible connections are recognized to be tenuous, for instance the Aref–Jones flow is two dimensional and slow, whereas at transition the flow is already three dimensional. Furthermore, in the shear layer flow the fluid motions themselves are free to evolve in time.

VI. CONCLUDING REMARKS

Since the major conclusions were anticipated in the Introduction, they need not be repeated here. The following are several closing comments. Independently of the validity or usefulness of the modeling approaches discussed here, the experimental data presented in the opening sections suggest the need for additional experimental and numerical investigations in which all relevant scales can be resolved for a range of Reynolds and Schmidt numbers. Effects of changes in Schmidt number are especially revealing, and, as the preceding sections indicate, the data are limited. The consequences of changes in these parameters observed in the experiments also imply that their variation in chaotic advection studies could be important, as the Aref–Jones study illustrates.

Perhaps one of the more interesting questions raised in the paper is the nature of the singularity $\mathrm{Re} \to \infty$ at fixed Schmidt number. The proposed behavior discussed in the text is based largely on intuitive arguments; a rigorous treatment would be most instructive.

Note added in proof. The stirring–mixing distinction was suggested by C. Eckart in Journal of Marine Research, VII, 3, 265 (1948). The da Vinci quotation in the Introduction appears in *An Introduction to Hydrodynamics and Water Waves*, by B. Le Méhauté (Springer-Verlag, New York, 1976).

ACKNOWLEDGMENTS

The authors are pleased to acknowledge helpful discussions with R. W. Dibble, A. R. Kerstein, and with their colleagues and students at Caltech and Stanford. They also thank M. Koochesfahani for providing the unpublished data in Fig. 11.

J. E. B. was supported under AFOSR Contract No. 90-

0304, ONR Grant No. N-00014-89-J-1991, and by the Gas Research Institute under Grant No. 5087-260-1467.

[1] H. Aref and S. W. Jones, Phys. Fluids A **1**, 470 (1989).
[2] G. L. Brown and A. Roshko, J. Fluid Mech. **64**, 775 (1974).
[3] P. E. Dimotakis and G. L. Brown, J. Fluid Mech. **78**, 535 (1976).
[4] M. G. Mungal, J. C. Hermanson, and P. E. Dimotakis, AIAA J. **23**, 1418 (1985).
[5] N. T. Clemens and M. G. Mungal, AIAA Paper No. AIAA-90-1978, 1990.
[6] L. P. Bernal and A. Roshko, J. Fluid Mech. **170**, 499 (1986).
[7] N. T. Clemens, Ph. D. thesis, Stanford University, Stanford, California, 1991.
[8] C. D. Winant and F. K. Browand, J. Fluid Mech. **63**, 237 (1974).
[9] A. K. M. F. Hussain, J. Fluid Mech. **173**, 303 (1986).
[10] H. E. Fiedler, Adv. Geophys. **18A**, 93 (1974).
[11] D. Oster and I. Wygnanski, J. Fluid Mech. **123**, 91 (1982).
[12] R. E. Breidenthal, J. Fluid Mech. **109**, 1 (1981).
[13] S. M. Masutani and C. T. Bowman, J. Fluid Mech. **172**, 93 (1986).
[14] C.-M. Ho and L. S. Huang, J. Fluid Mech. **119**, 443 (1982).
[15] J. C. Lasheras and H. Choi, J. Fluid Mech. **189**, 53 (1988).
[16] T. J. O'Hern, J. Fluid Mech. **215**, 365 (1990).
[17] R. E. Breidenthal, Phys. Fluids **23**, 1929 (1980).
[18] I. Wygnanski, D. Oster, H. Fiedler, and B. Dziomba, J. Fluid Mech. **93**, 325 (1979).
[19] D. Coles, Proc. Ind. Acad. Sci. (Eng. Sci.) **4**, 111 (1981).
[20] G. M. Corcos, in *Perspectives in Fluid Mechanics, Lecture Notes in Physics*, edited by D. Coles (Springer, Berlin, 1988). Vol. 320, p. 48.
[21] W. J. A. Dahm and P. E. Dimotakis, AIAA J. **25**, 1216 (1987).
[22] I. van Cruyningen, A. Lozano, and R. K. Hanson, Exp. Fluids, **10**, 41 (1990).
[23] M. G. Mungal, A. Lozano, and I. van Cruyningen, to appear in Exp. Fluids.
[24] R. A. Drebin, L. Carpenter, and P. Hanrahan, Comput. Graphics, **22**, 65 (1988).
[25] I. van Cruyningen, A. Lozano, M. G. Mungal, and R. K. Hanson, AIAA J. **29**, 479 (1991).
[26] A. E. Perry and T. T. Lim, J. Fluid Mech. **88**, 451 (1978).
[27] R. A. Antonia, A. Prabhu, and S. E. Stephenson, J. Fluid Mech. **72**, 455 (1975).
[28] R. Chevray and N. K. Tutu, J. Fluid Mech. **88**, 133 (1978).
[29] S. Komori and H. Ueda, J. Fluid Mech. **152**, 337 (1985).
[30] J. Tso, L. S. G. Kovasznay, and A. K. M. F. Hussain, J. Fluids Eng. **103**, 503 (1981).
[31] W. M. Pitts, Combust. Flame **76**, 197 (1989).
[32] P. E. Dimotakis, R. Miake-Lye, and D. A. Papantoniou, Phys. Fluids **26**, 3185 (1983).
[33] D. J. Shlien, J. Fluid. Mech. **183**, 163 (1987).
[34] M. G. Mungal and D. K. Hollingsworth, Phys. Fluids A **1**, 1615 (1989).
[35] J. H. Konrad, Ph. D. thesis, California Institute of Technology, Pasadena, California, 1976.
[36] G. L. Brown, *Fifth Australasian Conference on Hydraulics and Fluid Mechanics* (University of Canterbury, New Zealand, 1974), p. 352.
[37] P. E. Dimotakis, AIAA J. **24**, 1791 (1986).
[38] M. M. Koochesfahani and P. E. Dimotakis, J. Fluid Mech. **170**, 83 (1986).
[39] W. Kollmann and J. Janicka, Phys. Fluids **25**, 1755 (1982).
[40] R. G. Batt, J. Fluid Mech. **82**, 53 (1977).
[41] S. B. Pope, Combust. Sci. Technol. **25**, 159 (1981).
[42] M. G. Mungal and P. E. Dimotakis, J. Fluid Mech. **148**, 349 (1984).
[43] M. G. Mungal and C. E. Frieler, Combust. Flame **71**, 23 (1988).
[44] H. C. Hottel, *Proceedings of 4th Symposium (International) on Combustion* (The Combustion Institute, Pittsburgh, PA, 1953), p. 97.
[45] W. J. A. Dahm, P. E. Dimotakis, and J. E. Broadwell, AIAA Paper No. 84-0369, 1984.
[46] F. P. Ricou and D. B. Spalding, J. Fluid Mech. **11**, 21 (1961).
[47] W. J. A. Dahm, Ph. D. thesis, California Institute of Technology, Pasadena, California, 1985.
[48] J. E. Broadwell, in *Turbulent Reactive Flows, Lecture Notes in Engineering*, edited by R. Borghi and S. N. B. Murthy (Springer, Berlin, 1989), Vol. 40, p. 257.
[49] D. R. Dowling and P. E. Dimotakis, J. Fluid Mech. **218**, 109 (1990).
[50] M. G. Mungal and J. M. O'Neil, Combust. Flame **78**, 377 (1989).
[51] M. G. Mungal, P. S. Karasso, and A. Lozano, Combust. Sci. and Technol. **76**, 165 (1991).
[52] D. A. Papantoniou and E. J. List, J. Fluid Mech. **209**, 151 (1989).
[53] R. W. Dibble, M. B. Long, and K. Lyons (private communication).
[54] M. S. Uberoi and P. I. Singh, Phys. Fluids **18**, 764 (1975).
[55] P. H. Austin, M. B. Baker, A. M. Blyth, and J. B. Jensen, J. Atmos. Sci. **42**, 1123 (1985).
[56] R. A. Antonia, A. J. Chambers, D. Britz, and L. W. B. Browne, J. Fluid Mech. **172**, 211 (1986).
[57] C. H. Gibson, C. A. Friehe, and S. O. McConnell, Phys. Fluids **20**, S156 (1977).
[58] D. R. Dowling, Ph. D. thesis, California Institute of Technology, Pasadena, California, 1988.
[59] I. van Cruyningen, Ph. D. thesis, Stanford University, Stanford, California, 1990.
[60] C.-H. P. Chen and R. F. Blackwelder, J. Fluid Mech. **89**, 1 (1978).
[61] C. W. Van Atta, Arch. Mech. **29**, 161 (1977).
[62] C. W. Van Atta, in *Structure and Mechanisms of Turbulence II, Lecture Notes in Physics*, edited by H. Fiedler (Springer, Berlin, 1978), Vol. 76, p. 138.
[63] J. E. Broadwell and R. E. Breidenthal, J. Fluid Mech. **125**, 397 (1982).
[64] J. E. Broadwell and M. G. Mungal, *22nd (International) Symposium on Combustion* (The Combustion Institute, Pittsburgh, PA, 1988), p. 579.
[65] G. K. Batchelor, J. Fluid Mech. **5**, 113 (1959).
[66] P. E. Dimotakis, in Ref. 48, p. 417.
[67] P. G. Saffman, in *Topics in Nonlinear Physics*, edited by N. J. Zabusky (Springer, Berlin, 1968), p. 567.
[68] A. E. Lutz, R. W. Dibble, R. J. Kee, and J. E. Broadwell, AIAA Paper No. 91-0478, 1991.
[69] J. E. Broadwell, W. J. A. Dahm and M. G. Mungal, *20th (International) Symposium on Combustion* (The Combustion Institute, Pittsburgh, PA, 1984), p. 303.
[70] W. J. A. Dahm and R. W. Dibble, in Ref. 64, p. 801.
[71] M. F. Miller, C. T. Bowman, J. A. Miller, and R. J. Kee, Paper No. 89-110, Western States Section/The Combustion Institute, Fall Meeting, 1989.
[72] E. Effelsberg and N. Peters, Combust. Flame **50**, 351 (1983).
[73] J. C. LaRue and P. A. Libby, Phys. Fluids **17**, 1956 (1974).
[74] A. R. Kerstein, Combust. Sci. Technol. **60**, 392 (1988).
[75] A. R. Kerstein, Combust. Flame **75**, 397 (1989).
[76] A. R. Kerstein, J. Fluid Mech. **216**, 411 (1990).
[77] A. R. Kerstein, R. W. Dibble, M. B. Long, B. Yip, and K. Lyons, in *Seventh Symposium on Turbulent Shear Flows* (Stanford University, Stanford, 1989), Paper No. 14-2.
[78] H. Aref, J. Fluid Mech. **143**, 1 (1984).
[79] J. M. Ottino, *The Kinematics of Mixing: Stretching, Chaos and Transport* (Cambridge U.P., Cambridge, 1989).
[80] A. Leonard, V. Rom-Kedar, and S. Wiggins, Nucl. Phys. B (Proc. Suppl.) **2**, 179 (1987).
[81] *Disorder and Mixing*, NATO ASI Series E: Applied Sciences, edited by E. Guyon, J.-P. Nadal, and Y. Pomeau (Kluwer Academic, Dordrecht, The Netherlands, 1988), Vol. 152, p. 339.
[82] W. J. A. Dahm and K. A. Buch, in Ref. 77, Paper No. 14-1.
[83] C. W. Leong and J. M. Ottino, J. Fluid Mech. **209**, 463 (1989).
[84] L.-S. Huang and C.-M. Ho, J. Fluid Mech. **210**, 475 (1990).
[85] R. D. Moser and M. M. Rogers, Phys. Fluids A **3**, 1128 (1991).